

## RESEARCH ARTICLE SUMMARY

## MOLECULAR MOTORS

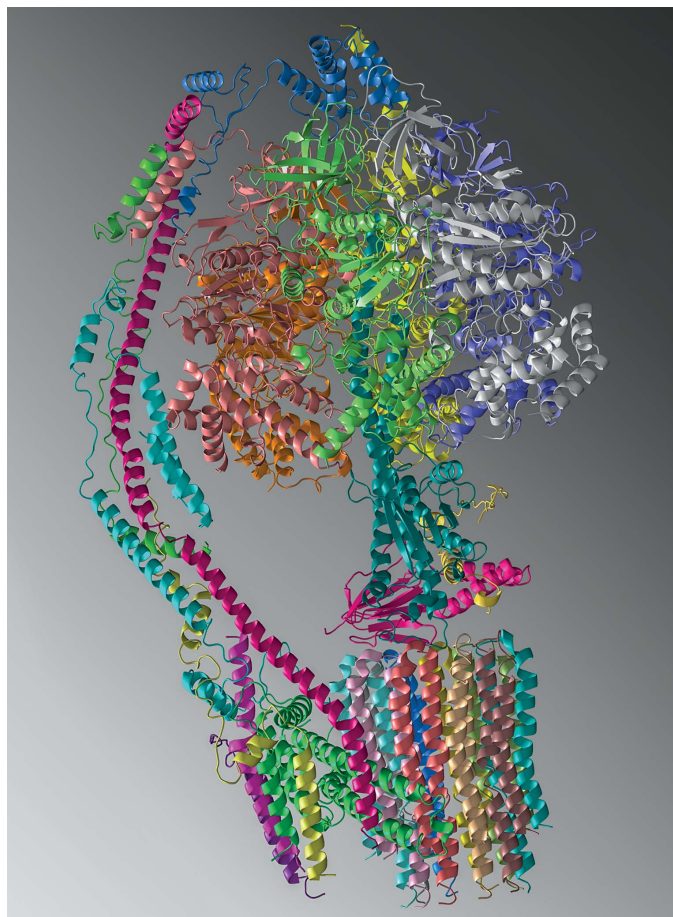
# High-resolution cryo-EM analysis of the yeast ATP synthase in a lipid membrane

Anurag P. Srivastava,\* Min Luo,\* Wenchang Zhou, Jindrich Symersky, Dongyang Bai, Melissa G. Chambers, José D. Faraldo-Gómez, Maofu Liao,† David M. Mueller†

**INTRODUCTION:** The mitochondrial adenosine triphosphate (ATP) synthase is the enzyme responsible for the synthesis of more than 90% of the ATP produced by mammalian cells under aerobic conditions. The chemiosmotic mechanism, proposed by Peter Mitchell, states that the enzyme transduces the energy of a proton gradient, generated by the electron transport chain, into the major energy currency of the cell, ATP. The enzyme is a large (about 600,000 Da, in the monomer state) multisubunit complex, with a water soluble complex ( $F_1$ ) that contains three active sites and a membrane complex ( $F_o$ ) that contains the proton translocation pathway, principally comprised of the  $a$  subunit and a ring of 10  $c$  subunits, the  $c_{10}$ -ring (10 in yeast, 8 in mammals).  $F_1$  has a central rotor that, at one end, is within the core of  $F_1$  and, at the other end, is connected to the  $c_{10}$ -ring of  $F_o$ . During ATP synthesis, the  $c_{10}$ -ring rotates, driven by the movement of protons from the cytosol to the mitochondrion, and in turn, the rotor rotates within  $F_1$  in steps of  $120^\circ$ . The rotation of the rotor causes conformational changes in the catalytic sites, which provides the energy for the phosphorylation of adenosine diphosphate (ADP), as first proposed in the binding-change hypothesis by Paul Boyer. The peripheral stalk acts as a stator connecting  $F_1$  with  $F_o$  and prevents the futile rotation of  $F_1$  as the rotor spins within it.

**RATIONALE:** Structural studies of the ATP synthase have made steady progress since the structure of the  $F_1$  complex was described in pioneering work by John Walker. However, obtaining a high-resolution

structure of the intact ATP synthase is challenging because it is inherently dynamic. To overcome this conformational heterogeneity, we locked the yeast mitochondrial rotor in a



**Structure of the monomeric yeast ATP synthase, as determined by cryo-EM, shown as a ribbon diagram.** The subunits are shown in different colors. The  $F_1$  complex is located at the top center and is composed of six subunits forming a nearly spherical structure and three subunits comprising the central stalk, or rotor. The  $F_o$  complex is located at the bottom, with the identity of the  $c_{10}$ -ring clearly seen. The peripheral stalk, or stator, is on the left, and the rotor is in the center of the molecule, extending into  $F_1$ .

single conformation by fusing a subunit of the stator with a subunit of the rotor, also called the central stalk. The engineered ATP synthase was expressed in yeast and reconstituted into nanodiscs. This facilitated structure determination by cryo-electron microscopy (cryo-EM) under near native conditions.

**RESULTS:** Single-particle cryo-EM enabled us to determine the structures of the membrane-

## ON OUR WEBSITE

Read the full article at <http://dx.doi.org/10.1126/science.aas9699>

embedded monomeric yeast ATP synthase in the presence and absence of the inhibitor oligomycin at 3.8- and 3.6-Å resolution, respectively. The fusion between the rotor and stator

caused a twisting of the rotor and a  $9^\circ$  rotation of the  $c_{10}$ -ring, in the direction of ATP synthesis, relative to the putative resting state. This twisted conformation likely represents an intermediate state in the ATP synthesis reaction cycle. The structure also shows two proton half-channels formed largely by the  $a$  subunit that abut the  $c_{10}$ -ring and suggests a mechanism that couples transmembrane proton movement to  $c_{10}$ -ring rotation. The cryo-EM density map indicates that oligomycin is bound to at least four sites on the surface of the  $F_o$   $c_{10}$ -ring that is exposed to the lipid bilayer; this is supported by binding free-energy molecular dynamics calculations. The sites of oligomycin-resistant mutations in the  $a$  subunit suggest that changes in the side-chain configuration of the  $c$  subunits at the  $a$ - $c$  subunit interface are transmitted through the entire  $c_{10}$ -ring.

**CONCLUSION:** Our results provide a high-resolution structure of the complete monomeric form of the mitochondrial ATP synthase. The structure provides an understanding of the mechanism of inhibition by oligomycin and suggests how extragenic mutations can cause resistance to this inhibitor. The approach presented in this study paves the way for structural characterization of other functional states of the ATP synthase, which is essential for understanding its functions in physiology and disease. ■

The list of author affiliations is available in the full article online.

\*These authors contributed equally to this work.

†Corresponding author. Email: david.mueller@rosalindfranklin.edu (D.M.M.); maofu\_liao@hms.harvard.edu (M.L.)

Cite this article as A. P. Srivastava et al., *Science*, 360, eaas9699 (2018).

DOI: 10.1126/science.aas9699

## RESEARCH ARTICLE

## MOLECULAR MOTORS

# High-resolution cryo-EM analysis of the yeast ATP synthase in a lipid membrane

Anurag P. Srivastava,<sup>1\*</sup> Min Luo,<sup>2\*</sup> Wenchang Zhou,<sup>3</sup> Jindrich Symersky,<sup>1</sup> Dongyang Bai,<sup>1</sup> Melissa G. Chambers,<sup>2</sup> José D. Faraldo-Gómez,<sup>3</sup> Maofu Liao,<sup>2†</sup> David M. Mueller<sup>1†</sup>

Mitochondrial adenosine triphosphate (ATP) synthase comprises a membrane embedded  $F_0$  motor that rotates to drive ATP synthesis in the  $F_1$  subunit. We used single-particle cryo-electron microscopy (cryo-EM) to obtain structures of the full complex in a lipid bilayer in the absence or presence of the inhibitor oligomycin at 3.6- and 3.8-angstrom resolution, respectively. To limit conformational heterogeneity, we locked the rotor in a single conformation by fusing the F6 subunit of the stator with the  $\delta$  subunit of the rotor. Assembly of the enzyme with the F6- $\delta$  fusion caused a twisting of the rotor and a 9° rotation of the  $F_0$   $c_{10}$ -ring in the direction of ATP synthesis, relative to the structure of isolated  $F_0$ . Our cryo-EM structures show how  $F_1$  and  $F_0$  are coupled, give insight into the proton translocation pathway, and show how oligomycin blocks ATP synthesis.

The mitochondrial adenosine triphosphate (ATP) synthase is composed of two distinct molecular motors,  $F_1$  and  $F_0$  (Fig. 1 and Movie 1).  $F_1$  includes three catalytic subunits around a central rotor that rotates to effect ATP synthesis.  $F_0$  is a transmembrane proton turbine that includes the  $c_{10}$ -ring, a ring of 10  $c$  subunits, which rotates in steps of 36° as it moves protons from the cytosol to the matrix space, down an electrochemical gradient (1). The  $c_{10}$ -ring in  $F_0$  is physically coupled to the rotor in  $F_1$ , and therefore, proton translocation drives the synthesis of ATP.  $F_1$  is held in place by a peripheral stator that prevents the rotation of the body of  $F_1$  and restricts the wobbling of its central rotor relative to the  $c_{10}$ -ring. Relative to the stator, the  $F_1$  rotor can be in three distinct positions (rotomers), whereas a revolution of the  $c_{10}$ -ring involves 10 discrete steps. This combination of 120° steps of the rotor and 36° steps of the  $c_{10}$ -ring results in multiple conformations of the ATP synthase during the reaction cycle. Furthermore, the ATP synthase can form homodimers (2–4), which further increases the number of possible conformations of the enzyme complex, making the analysis of the reaction mechanism

on a molecular level challenging. Here we have used a genetic method to restrict the number of conformations, allowing us to study the monomeric form of the yeast ATP synthase. We reconstituted the monomeric enzyme complex into a lipid bilayer formed in nanodiscs to enable structural analysis under near native conditions.

To restrict the number of conformations, we genetically fused subunit F6 of the stator to the  $\delta$  subunit of the rotor. The subunits were linked by T4 lysozyme, giving a final fusion of  $H_2N$ -F6-lysozyme- $\delta$ - $CO_2H$  (fig. S1). The mitochondrial leader peptide from the  $\beta$  subunit (ATP2) was added to direct the import of the protein into the mitochondria, and the expression was controlled with the ATP2 transcriptional elements. The plasmid containing this fusion was integrated into the genome of a yeast strain that is devoid of the genes encoding F6 (ATP14) and the  $\delta$  subunit (ATP16). The gene encoding ATP2 was also deleted in the strain, but this was complemented by integration of a vector into the genome that contains the  $\beta$  subunit with a His<sub>6</sub> tag on the amino terminus, allowing rapid purification of the enzyme.

We performed single-particle cryo-electron microscopy (cryo-EM) analysis on the nanodisc-reconstituted ATP synthase both with and without the inhibitor oligomycin. Three preparations of nanodiscs (5) were used, which differed in their lipid content (see methods). Overall, the cryo-EM density that gave rise to the model of the  $F_1F_0$  ATP synthase was more complete under the conditions with oligomycin than without, but the structures were similar. Thus, we will confine the discussion of the overall structure to the structure with bound oligomycin.

To allow analysis of the proton translocation mechanism, the refinement was focused on  $F_0$ , which improved resolution of this region but also resulted in poorer resolution of the other parts of the enzyme. For the  $F_0$  regions, we compare the structures with and without bound oligomycin.

## Overall structure of the ATP synthase

The cryo-EM structures of the yeast ATP synthase in nanodiscs were determined to overall resolutions of 3.6- and 3.8-Å for the entire enzyme complex in the absence or presence of oligomycin, respectively (see Fig. 2, Table 1, and figs. S1 to S5). The EM density for  $F_0$  is weaker and of lower resolution than that of  $F_1$ , likely owing to flexibility between these domains. Hence,  $F_0$ -focused three-dimensional (3D) classification and refinement improved the resolution and map quality. In the presence of oligomycin, the flexibility of the ATP synthase was reduced, resulting in better EM density for  $F_0$  and the stator and a greater number of residues in  $F_0$  with well-defined side-chain densities. The resolution varied between subunits and within subunits. Most residues in the  $F_1$  subunits display excellent side-chain density, whereas the stator and  $F_0$  subunits showed varying resolutions. Many good side-chain densities could be seen for most of the components present in the cryo-EM structures, including the central stalk and  $c_{10}$ -ring. The secondary structural elements are also well resolved for the stator components. We were able to trace 27 chains in the density (Fig. 3A, Movie 2, and Table 2). The only chains that we did not see are those involved in dimerization of the ATP synthase (as this is the monomer form). The density for the T4 lysozyme molecule used to fuse F6

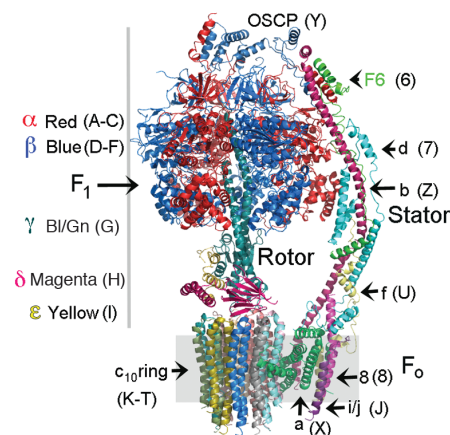


**Fig. 1. Subunit composition and architecture of the monomeric yeast ATP synthase.**

The subunits are shown in a variety of colors to allow identification. The chain number or letter used in the PDB code is shown in parentheses. There are three  $\alpha$  (red) and three  $\beta$  (blue) subunits that, with the  $\gamma$  (bl/gn, blue-green),  $\delta$  (magenta), and  $\epsilon$  (yellow) subunits, form  $F_1$ . The rotor is comprised of the  $\gamma$ ,  $\delta$ , and  $\epsilon$  subunits of  $F_1$ . The core of  $F_0$  is comprised of the  $a$  subunit and the  $c_{10}$ -ring. The subunits of the stator are as shown.

<sup>1</sup>Department of Biological Chemistry and Molecular Biology, Chicago Medical School, Rosalind Franklin University, 3333 Green Bay Road, North Chicago, IL 60064, USA.

<sup>2</sup>Department of Cell Biology, Harvard Medical School, 250 Longwood Avenue, SGM 509, Boston, MA 02115, USA.

<sup>3</sup>Theoretical Molecular Biophysics Laboratory, National Heart, Lung, and Blood Institute, National Institutes of Health, 50 South Drive, Bethesda, MD 20892, USA.

\*These authors contributed equally to this work.

†Corresponding author. Email: david.mueller@rosalindfranklin.edu (D.M.M.); maofu\_liao@hms.harvard.edu (M.Li.)



with  $\delta$  is seen in one of the cryo-EM maps from 3D classification (fig. S3C). Low-resolution density for the lipid nanodisc clearly delineates the membrane-embedded regions of  $F_o$  (Fig. 2).

There are three catalytic sites in  $F_1$ , each of which cycles between three states. In the first high-resolution crystal structure of the  $F_1$  ATPase, the sites were occupied with adenosine diphosphate (ADP) or ATP and one site was empty, and thus they were named DP, TP, and E, respectively (Table 2) (6). The asymmetry of the catalytic sites is determined by the relative position of the  $\gamma$  subunit within  $F_1$ . In our cryo-EM structures, the rotor is in a single orientation, and the asymmetry of the catalytic sites is conserved. In this orientation, the stator bridges  $F_o$  with  $F_1$  along the noncatalytic site formed by chains B ( $\alpha_{TP}$ ) and E ( $\beta_{DP}$ ). There is contact between subunit d of the stator with  $\alpha_{TP}$  (chain B).

The  $F_1$  domain

The conformation of the yeast  $F_1$  domain in the cryo-EM structures is nearly identical to that observed in the crystal structures of yeast  $F_1$  (7) or yeast  $F_1$ -c10 (8, 9), which also revealed the three distinct states of the catalytic sites DP, TP, and E. When we superimpose yeast  $F_1$  onto the structure of yeast  $F_1F_o$ , we see that the rotor formed by the  $\gamma$ ,  $\delta$ , and  $\epsilon$  subunits is twisted by about 9° in the direction of the rotation that leads to ATP synthesis (Fig. 3B). The twisting starts at about  $\gamma$ -Ile<sup>271</sup>, which is in direct contact with the collar formed by the  $\alpha$  and  $\beta$  subunits (6). At the bottom of the rotor, this twisting results in a displacement of about 5.6 Å in residues in the  $\delta$  subunit. This displacement continues into the c10-ring and causes a commensurate rotation of the c10-ring relative to the a subunit in  $F_o$  (Fig. 3C). Although we believe that the constraint of the central stalk with the stator can mimic the twisting of the central stalk during the reaction cycle, this is a first approximation and has not been proven.

The stator domain

The stator (peripheral stalk) is composed of subunits OSCP (oligomycin sensitivity conferral protein), b, d, F6, f, i/j, and 8. Subunits OSCP, b, d, f, and F6 primarily serve as structural components of the stator. However, subunits b, d, f, i/j, and 8 are either embedded or attached to the membrane and are part of the complex purified as  $F_o$ ; they may have a role in proton movement in addition to a structural role in forming the stator. Subunits b and d are similar to their homologs in the crystal structure of bovine subunits F6, b, and d [Protein Data Bank (PDB) 2CLY] (10); however, yeast F6 displays differences from bovine F6, including an additional helix (residues 76 to 91) at the C terminus, which adds additional interactions with the b and d subunits. Modeling of the domains of stator subunits that are part of  $F_o$  and embedded or bound to the membrane was aided by the high-resolution cryo-EM structure of yeast  $F_o$  (PDB 6B2Z) (11), and we did not see any major differences as compared to the reported structure.

The OSCP subunit anchors the stator at the top of  $F_1$ . As partially seen in the structure of the enzyme from the yeast *Pichia angusta* (12),

the N terminus of the three  $\alpha$  subunits interact to stabilize the binding of OSCP to the top of  $F_1$  (fig. S7). The helix in  $\alpha_{TP}$  (chain B) formed from BLys<sup>4</sup> to BAsn<sup>26</sup> interacts with helices from F6 and the b subunit (fig. S7, region I). Furthermore, the three-helix bundle formed by residues B462 to B509 interact with two helices of the d subunit from residues 3 to 48, and a cluster of residues in OSCP ranging from 160 to 168 as well as resi-

due 122 (region I). Residues in a random coil from  $\alpha_{DP}$  (chain C, Gln<sup>6</sup> to Ser<sup>22</sup>) run under and interact with OSCP (fig. S7, region III). The helix formed from residues Lys<sup>4</sup> to Lys<sup>19</sup> in  $\alpha_E$  (chain A) interacts with a helix and turn in OSCP formed by residues Thr<sup>46</sup> to His<sup>78</sup> (fig. S7, region IV). Thus, the N terminus of each  $\alpha$  subunit makes specific contributions to the stabilization of the anchoring of OSCP to the top of  $F_1$ .

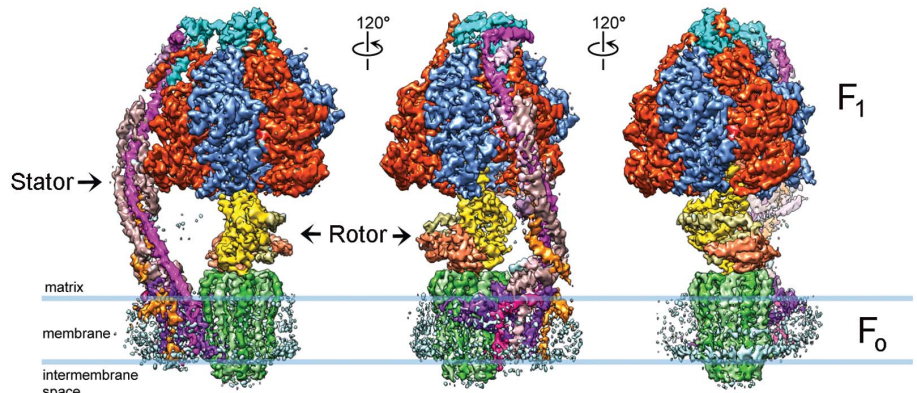


**Fig. 2. Cryo-EM 3D reconstruction of nanodisc-embedded yeast ATP synthase bound with oligomycin.** Three side views of the 3D reconstruction filtered to 3.8-Å resolution and rotated by 120° around the y axis. All subunits are differently colored. Blue lines indicate the membrane boundaries, as observed by the EM density of the lipid nanodisc.

Table 1. Statistics of the cryo-EM structures presented in this study.				
Category	ATP synthase		ATP synthase with oligomycin	
Cryo-EM data collection and processing				
Electron microscope	Polara		Polara	
Voltage (kV)	300		300	
Electron dose (e <sup>-</sup> /Å <sup>2</sup> )	41		41	
Physical pixel (Å)	1.23		1.23	
Number of movies	5,935		2,896	
Number of particles	541,568		346,399	
	F <sub>1</sub> F <sub>o</sub>	F <sub>o</sub>	F <sub>1</sub> F <sub>o</sub>	F <sub>o</sub>
Number of particles for final map	160,937	109,206	104,280	104,280
Resolution (Å)	3.6	4.1	3.8	4.2
Map B-factor (Å <sup>2</sup> )	-100	-180	-100	-200
Model refinement				
Number of protein residues	5,094	1,224	5,094	1,224
Number of side chains	5,061	1,198	5,061	1,199
Number of atoms	38,814	9,179	38,814	9,434
Geometric parameters (root mean square deviation)				
Bond length (Å)	0.007	0.008	0.009	0.003
Bond angle (°)	1.026	1.309	1.119	1.354
Ramachandran statistics				
Residues favored (%)	93.87	92.95	92.18	92.95
Residues allowed (%)	5.93	6.59	7.62	7.05
Residues disallowed (%)	0.20	0.46	0.20	0
Rotamer outliers (%)	0.15	3.23	0.36	0.21
MolProbity score	1.89	2.57	1.91	2.56
EMRinger score	1.61	0.94	1.55	0.91

## The F<sub>o</sub> domain

F<sub>o</sub> is embedded in the inner membrane of the mitochondria. Our cryo-EM map showed clear density for the lipid bilayer in the nanodiscs (Figs. 1 and 4A). The cryo-EM density indicates that the bilayer spans about 37 Å, approximately from Pro<sup>49</sup> to Phe<sup>74</sup> on the outer helices of the c subunits. Phe<sup>74</sup> is the last residue in helix 2 (residues 42 to 74) and is considerably shorter than helix 1 (residues 1 to 40).

The a subunit is adjacent to the c<sub>10</sub>-ring and contributes to form the proton-conduction pathway from the cytosolic side of the mitochondria to protonation sites in the c<sub>10</sub>-ring and from these sites to the matrix space (13–15). The protonation and deprotonation events at the interface between the a subunit and the c<sub>10</sub>-ring couple the translocation of protons to the rotation of the c<sub>10</sub>-ring and thus effect ATP synthesis. We obtained the near-atomic resolution F<sub>o</sub> maps for the enzyme without bound oligomycin and with oligomycin, and the structural models from these maps are nearly identical. This suggests that oli-

gomycin binding does not alter the overall structure of F<sub>o</sub>.

The structure of the c<sub>10</sub>-ring is nearly identical to that observed in a crystal structure of the isolated ring (16). (We have numbered the c subunits relative to the a subunit, with c<sup>1</sup>Glu<sup>59</sup> corresponding to the first c subunit that has interactions with the a subunit. The c subunits are numbered sequentially in the direction of rotation during ATP synthesis; refer to Fig. 3C.) Glu<sup>59</sup> is the proton acceptor and donor that is responsible for net proton movement during the catalytic cycle. The side chain of Glu<sup>59</sup> has been shown to be in one of two conformations: a “closed” conformation, which was suggested to represent the protonated form when in the membrane, and an “open” conformation, which was proposed to be present only at the a-c interface and to represent the state in which protonation and deprotonation occurs (16, 17). We see four instances where Glu<sup>59</sup> is in the open conformation in the membrane phase, suggesting that the closed conformation is not a necessary conforma-

tion of the protonated side chain in the membrane phase (fig. S8).

The structure of dimeric yeast F<sub>o</sub> was solved by cryo-EM after stripping off F<sub>1</sub> by using NaBr (11). This structure likely represents the “ground state,” as it is free from strain caused by assembly of the F<sub>1</sub>F<sub>o</sub> ATP synthase complex. We superimposed the F<sub>o</sub> region from the ground state onto the F<sub>o</sub> region from our native structures using the a and b subunits as the anchor (Fig. 3C). This analysis indicates that the c<sub>10</sub>-ring of the native structure, relative to the a subunit, is rotated about 9° in the direction of ATP synthesis, as compared to the ground state. This is consistent with the rotation that we observed in the F<sub>1</sub> rotor, when comparing our structure to that of F<sub>1</sub> alone.

Arg<sup>176</sup> of the a subunit is the only residue that is strictly conserved (13) (fig. S9). It has been proposed that Arg<sup>176</sup> prevents the short-circuiting of protons in the proton pathway (18) as well as acting as a positive pole for attraction of the charged Glu<sup>59</sup> (14). In the isolated F<sub>o</sub> structure (11) (the ground state structure), atoms in the corresponding side chains of Arg<sup>176</sup> and the closest Glu<sup>59</sup> (c<sup>2</sup>Glu<sup>59</sup>) are separated by 5 to 7.5 Å, whereas in our structure, the side chains move closer, to within 3.8 Å (Fig. 3D). Extrapolation on the movement of the c<sub>10</sub>-ring in the direction of ATP synthesis would predict an even closer configuration of Arg<sup>176</sup> and Glu<sup>59</sup>, thereby creating a potential contributing force for rotation of the c<sub>10</sub>-ring. This attractive force will be much reduced once the ionized cGlu<sup>59</sup> is protonated.

## The proton pathway

During ATP synthesis, protons transit from the cytosolic side of the mitochondrial membrane to protonate the c-subunit Glu<sup>59</sup> closest to Arg<sup>176</sup> (c<sup>2</sup>Glu<sup>59</sup>), thereby releasing this interaction. Protons must be released from c<sup>1</sup>Glu<sup>59</sup> into the matrix space (Fig. 4A), although not necessarily in concert with protonation, enabling this side chain to engage Arg<sup>176</sup> following a 36° step. The hydrophilic spaces that provide pathways for protons from the cytosol and then to the matrix space, allowing protonation and later deprotonation of cGlu<sup>59</sup>, are referred to as half-channels. Figure 4 and Movie 3 show the putative half-channels from the cytoplasm and to the matrix. Their location and identification is consistent with recent reports (11, 19–21). The matrix-side half-channel is most obvious at the a-c interface, where the side chains of a number of residues appear to form a hydrophilic cavity that extends from c<sup>1</sup>Glu<sup>59</sup> to the surface of the membrane phase (Fig. 4, A, C, and D). aGlu<sup>162</sup> is an important, but not essential, residue in this pathway (13). The matrix half-channel extends up to the point that we have determined to be the edge of the membrane. By contrast, the cytoplasmic half-channel is formed by residues in the f, b, and a subunits. The proton-conduction pathway appears to include aHis<sup>185</sup> and aGlu<sup>223</sup> (Fig. 4, A and B). The proton-conduction pathway proceeds between helices 5 and 6 of the a subunit. aHis<sup>185</sup> and aGlu<sup>223</sup> are interchanged in the enzymes from other species but remain in comparable positions (fig. S9). The protonation of cGlu<sup>59</sup> likely

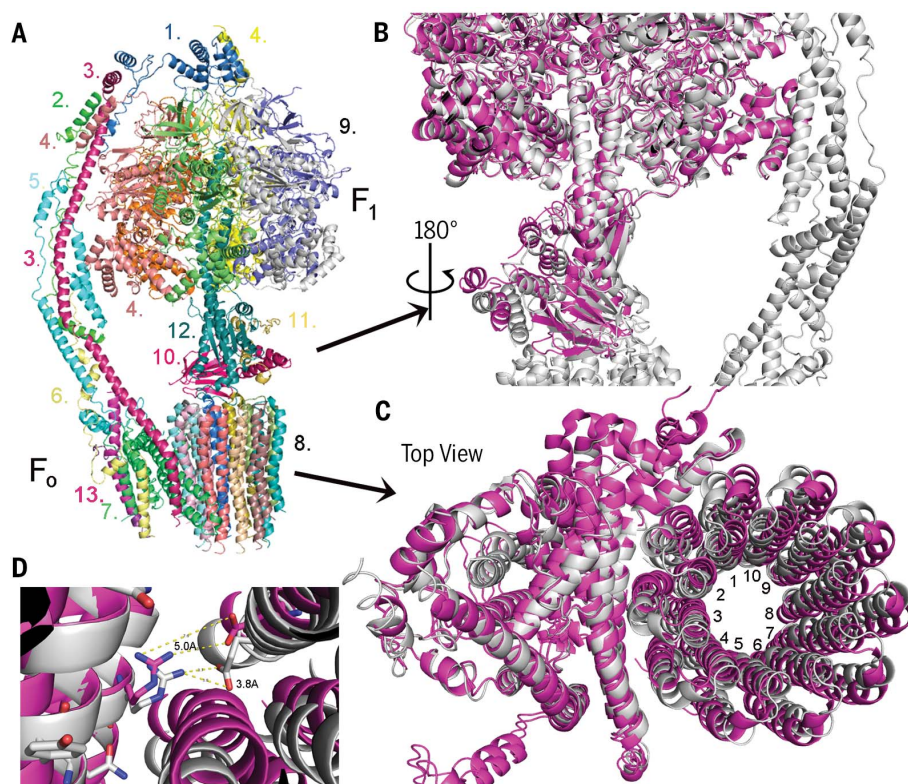


**Fig. 3. Overall structure of the yeast ATP synthase.** (A) Molecular model of the F<sub>1</sub>F<sub>o</sub> ATP synthase based on the cryo-EM density map. The subunits are color coded and labeled as follows: 1) OSCP, 2) F6, 3) b subunit, 4) α subunit, 5) d subunit, 6) f subunit, 7) a subunit, 8) c<sub>10</sub>-subunit ring, 9) α<sub>3</sub>β<sub>3</sub> core, 10) δ subunit, 11) ε subunit, 12) γ subunit, and 13) i/j subunit. (B) Superimposition of the crystal structure of the yeast F<sub>1</sub> domain (magenta) onto the cryo-EM structure of yeast F<sub>1</sub>F<sub>o</sub> ATP synthase (gray). Three rotor subunits (γ, δ, and ε subunits) are displaced by a twisting in the counterclockwise direction. (C) Superimposition of the cryo-EM structure of yeast F<sub>o</sub> (magenta, in the absence of F<sub>1</sub>) onto the current structure of F<sub>1</sub>F<sub>o</sub> (gray). The c<sub>10</sub>-ring is rotated by about 9° in the counterclockwise direction (the direction of ATP synthesis). The numbers indicate the c subunits numbered sequentially in the direction of rotation during ATP synthesis, relative to the a subunit. (D) Relative position of aArg<sup>176</sup> and the nearest cGlu<sup>59</sup> in the structure of yeast F<sub>o</sub> (magenta) and F<sub>1</sub>F<sub>o</sub> (gray). The distance between the side chains of aArg<sup>176</sup> and cGlu<sup>59</sup> is reduced from about 5.0 to about 3.8 Å with the rotation of the c<sub>10</sub>-ring by 9°.



occurs in the transition from c<sup>2</sup>Glu<sup>59</sup> to c<sup>3</sup>Glu<sup>59</sup> and, in doing so, eliminates any charge interaction between aArg<sup>176</sup> and cGlu<sup>59</sup>.

Possible role of aGlu<sup>162</sup> and aGlu<sup>223</sup>

A requirement for a proton donor or acceptor in the reaction pathway is that the value of the pK<sub>a</sub> (where K<sub>a</sub> is the acid dissociation constant) of the donor and acceptor should be around the pH of the medium. The pH of the cytosol is around 7.0, whereas that of the matrix space during active ATP synthesis is around 8.0. Thus, the pK<sub>a</sub> of the carboxyl of cGlu<sup>59</sup> should be around 7.0 at the a-subunit interface to be an effective proton carrier. If the pK<sub>a</sub> of the carboxyl was the standard value in water, 5.0, then the carboxyl would rarely be in the protonated state, and rotation would be severely impeded during ATP synthesis. Although a low pK<sub>a</sub> would allow the release of the proton to the matrix space during ATP synthesis, it would impede the reversal of the ATP synthase reaction—ATP hydrolysis—which is a fundamental feature of the enzyme. Thus, the pK<sub>a</sub> of the cGlu<sup>59</sup> must be around 7.0 at both the sites for protonation and deprotonation to occur during ATP synthesis and hydrolysis. Although there is a report that the pK<sub>a</sub> of the c-ring carboxylate is 7.0 (22), these measurements were not made under native conditions nor measured in the intact enzyme. On the basis of the structure, we suggest that aGlu<sup>162</sup> and aGlu<sup>223</sup> may play a role in shifting the pK<sub>a</sub> of cGlu<sup>59</sup>. Residue aGlu<sup>162</sup> is highly conserved across species. The corresponding residue in *Mycobacteria* is aGln<sup>172</sup>, but just one turn away is a pair of glutamate residues, thus functionally conserving the role of aGlu<sup>162</sup> (fig. S9). The cGlu<sup>59</sup> carboxyl nearest to aGlu<sup>162</sup> (c<sup>1</sup>Glu<sup>59</sup>) (Fig. 4B) is thus likely to be the proton-releasing site. Rotation of the c<sub>10</sub>-ring by about 9° places c<sup>1</sup>Glu<sup>59</sup> about 4 Å from aGlu<sup>162</sup> (fig. S10). On the cytosolic side, aGlu<sup>223</sup> is in a dyad interaction with aHis<sup>185</sup>, this pair is nearly strictly conserved and likely to serve as an intermediate proton-binding site (fig. S9). Rotation of the c<sub>10</sub>-ring by about 27°, facilitated by the deprotonation of c<sup>1</sup>Glu<sup>59</sup>, could bring c<sup>2</sup>Glu<sup>59</sup> close enough to interact with aGlu<sup>223</sup>, with multiple bridging water molecules. These interactions of aGlu<sup>162</sup> and aGlu<sup>223</sup> with the side chain of cGlu<sup>59</sup> have the potential to shift the pK<sub>a</sub> of the side-chain cGlu<sup>59</sup> up to around 7.0, where it needs to be to act as an effective proton-transfer group. There is precedence for glutamate-glutamate interactions and histidine-glutamate interactions altering the pK<sub>a</sub> of carboxylates to around 7.0 (23–26). This hypothesis is consistent with biochemical data that show that replacements at these two positions alter the magnitude of the potential gradient that the enzyme can create with the hydrolysis of ATP (13, 27, 28). Of course, this is still hypothetical, and proof will require the structure determination of multiple intermediate states of the reaction cycle.

Inhibition by oligomycin

The crystal structure of the isolated yeast c<sub>10</sub>-ring with bound oligomycin has been determined at

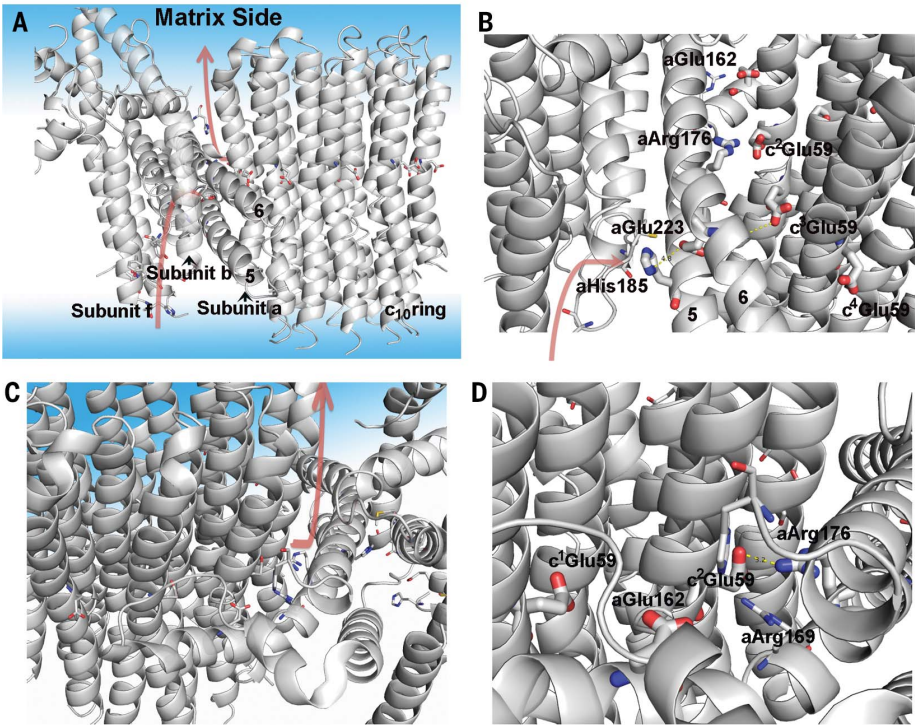


**Fig. 4. Model of F<sub>0</sub> and the proton pathways.** (A) Overall model of F<sub>0</sub> with subunits a, b, c, and f displayed. The aqueous phase is also displayed with a light blue coloring. The postulated proton pathways for the entry from the intermembrane space and exit to the matrix are shown with salmon-colored arrows. The protonation pathway during ATP synthesis is a path formed by subunits f, b, and a, with the final course formed by helices 5 and 6 (labeled) of the a subunit. (B) Side view of the entry pathway for protons during ATP synthesis, with key residues indicated (see text for discussion). (C) View from the top side of the proton pathway for proton exit to the matrix. (D) View of proton pathway from the exit site, showing helices 5 and 6 of the a subunit and the c<sub>10</sub>-ring.

Table 2. Summary of subunit composition, chain names, and residues in this model. The DP, TP, and E sites in F <sub>1</sub> are composed of chains C and D, B and F, and A and E, respectively.							
Subunit	Alias	Total number of residues	Molecular mass (kDa)	Role	Sector	Chain	Modeled residues
α		510	54.9	catalytic	F <sub>1</sub>	A to C	4 (or 6) to 510
β		478	51.1	catalytic	F <sub>1</sub>	D to F	6 (or 7) to 478
γ		278	30.6	catalytic	F <sub>1</sub>	G	1 to 278
δ		138	14.6	catalytic	F <sub>1</sub>	H	7 to 138
ε		61	6.1	catalytic	F <sub>1</sub>	I	1 to 59
OSCP		195	20.9	structural	stator	Y	7 to 172
a		249	25.1	H <sup>+</sup> transfer	F <sub>0</sub>	X	26 to 249
b		209	23.3	dual	F <sub>0</sub>	Z	53 to 207
c		76	7.76	H <sup>+</sup> transfer	F <sub>0</sub>	K to T	1 to 75 (or 76)
d		173	19.7	structural	stator	7	3 to 173
f		95	10.6	dual	F <sub>0</sub>	U	1 to 85
i	j	59	6.7	H <sup>+</sup> transfer	F <sub>0</sub>	J	1 to 37
F6		92	10.4	structural	stator	6	4 to 92
8	A6L	48	5.8	structural	stator	8	7 to 48

1.9 Å (PDB 4F4S) (29). Oligomycin was shown to bind to the c<sub>10</sub>-ring with the inhibitor spanning the outer helices of two adjacent c subunits and centered over cGlu<sup>59</sup>. It has been unclear whether oligomycin would bind to the c<sub>10</sub>-ring in a lipid

environment or to alternative sites in the ATP synthase. The cryo-EM analysis here shows densities at four sites on the c<sub>10</sub>-ring where we modeled four oligomycin molecules (oligo1 to oligo4) (spanning c<sup>2</sup>c<sup>6</sup>, c<sup>6</sup>c<sup>7</sup>, c<sup>7</sup>c<sup>8</sup>, and c<sup>8</sup>c<sup>9</sup>); these densities are

positioned in the membrane phase and at the same position where oligomycin was seen to bind in the crystal structure of the  $c_{10}$ -ring (29) (Fig. 5A). The density map for oligo1 to oligo4 suggests that there is some variation in the binding strength at each site. This may reflect slight differences in the conformation of the main and side chains at each binding site. There is also weak density at  $c^4c^5$ , which is at the edge of the a-c interface, but the best fit to the density with an oligomycin molecule (oligo5) places oligomycin in a much different binding mode as compared to those in the other sites (fig. S11). Furthermore, the conformation of oligo5, as modeled, is largely different from that observed previously. Likely, the weak density attributed to oligo5 is due in part to surrounding lipid molecules. Thus, we believe that this, at best, represents a minor binding mode.

To test the hypothesis that oligomycin can bind in a stable mode to the  $c_{10}$ -ring in a membrane environment, we evaluated the free energy of formation of this complex using all-atom molecular dynamics simulations (fig. S12). This binding free energy can be defined as  $\Delta G_b = -k_B T \ln N + \Delta G_{int} + \Delta G_r + \Delta G_t$ , where  $k_B$  is the Boltzmann constant,  $T$  is temperature,  $N$  is the number of available binding sites on the  $c_{10}$ -ring,  $\Delta G_{int}$  is the free-energy difference between the associated and dissociated complex, and  $\Delta G_r$  and  $\Delta G_t$

are the free-energy penalties due to the loss of rotational and translational entropy of the inhibitor upon binding, respectively. The values calculated from the simulation data are (detailed in methods)  $\Delta G_{int} = -6.6$  kcal/mol,  $\Delta G_r = +1.6$  kcal/mol, and  $\Delta G_t = +4.4$  kcal/mol, where the latter assumes that the mole fraction of oligomycin in the membrane is 0.01. For  $N = 7$  (that is, the number of c subunits exposed to the membrane), the resulting value of the binding free energy,  $\Delta G_b = -1.7$  kcal/mol, implies that oligomycin is about 20 times more likely to be bound to the  $c_{10}$ -ring than free in the lipid bilayer. (Note that  $\Delta G_t$  would be reduced for higher oligomycin densities, and thus binding would be more favorable. For a mole fraction of 0.05,  $\Delta G_t$  is +3.5 kcal/mol, and  $\Delta G_b$  would range from -2.7 kcal/mol for  $N = 7$  to -1.5 kcal/mol for  $N = 1$ , which translate into binding probabilities ranging from 90:1 to 10:1.) This energetic analysis hence supports the conclusion that oligomycin binds to the  $c_{10}$ -ring subunits exposed to the lipid bilayer. All available data therefore suggest that oligomycin inhibits the enzyme by first binding to the  $c_{10}$ -ring and thus impairs its rotation against subunit a. Likely, the c subunit with bound oligomycin is sterically prevented from entering the a-c interface, but, if it did, it would be unable to either release the bound proton or accept a proton during the catalytic cycle.

There are three sites reported in the a subunit where mutations cause yeast to be resistant to oligomycin. The mutations conferring resistance are Ile<sup>161</sup>→Met; Ser<sup>165</sup>→Thr, Cys, or Tyr; and Leu<sup>222</sup>→Phe (30). The sites are mapped onto the model for  $F_0$  (Fig. 5, B to D). This poses a paradox, in that these mutations map to locations that are separated by as many as 61 residues along a single  $\alpha$  helix and distant from the binding sites mapped on the  $c_{10}$ -ring. However, the resistance-forming residues all face the  $c_{10}$ -ring and are positioned almost at the center of the region where oligomycin is known to bind, though not at those specific sites. These bulky replacements in the a subunit will disrupt the  $c_{10}$ -ring at the point of their interaction but, in doing so, also disturb the interaction between the neighboring two c subunits. We propose that the disruption in the conformation of the  $c_{10}$ -ring, possibly just on the surface, is propagated through all c subunits, thereby allowing a stable  $c_{10}$ -ring and altering the conformation of all oligomycin binding sites. As such, the conformation of the wild-type c subunit (represented here as  $cO^S$ ) is converted to a conformation that is resistant to oligomycin,  $cO^R$ . However, for a  $c_{10}$ -ring to form, each subunit must have identical contacts between the  $c_{10}$ -ring, and thus  $c_1O^R c_9O^S$  gets converted to  $c_{10}O^R$  (where the subscript represents the number of c subunits) in the presence of the oligomycin-resistance mutation in the a subunit. This suggests that the conformation of the  $c_{10}$ -ring surface is plastic, in that it can assume new stable forms that allow it to function. This represents a mechanism that differs from allosteric interactions as they are normally thought of in relationship to enzyme regulation.

## Materials and methods

### Yeast strains and plasmids

Yeast wild type, USY006 (Mata, ade2-1, his3-11,15, leu2-1, trp1-1, ura3-52, atp2::LEU2, pRS304-ATP2H6::TRP1) and yeast with F68 fusion, DMY741 (Mata, ade2-1, his3-11,15, trp1-1, ura3-52, can1<sup>R</sup>100, atp2::loxP, atp7::loxP, atp1::KANR, F68::LEU2, ATP2-H6::TRP1, ATP1::URA3) were used throughout. pMSPIE3D1 (31) was a gift from Stephen Sligar (Addgene plasmid # 20066) and was transformed into BL21 (DE3) Gold (Agilent, Santa Clara, CA). Plasmid pRK792 (32) (to express TEV protease) was a gift from David Waugh (Addgene plasmid # 8830). The yeast was grown in a 60l fermentor in semisynthetic media with the glucose concentration controlled to about 0.2% (33). Bacteria were grown in LB media.

The parent strain for DMY741 was W303-1A (Rodney Rothstein via Alex Tzagoloff, Columbia University). Strain DMY741 was developed by sequentially deleting out the genes (34), ATP1, ATP2, ATP7, and ATP16 and then introducing the genes on plasmids containing ATP1, ATP2 with a His<sub>6</sub> tag, and the fusion construct contain subunit F6 (ATP7), T4-lysozyme, and the  $\delta$  subunit (ATP16). The fusion construct was made by total synthesis of the DNA (Genscript, Piscataway, NJ). The DNA sequence that encoding T4 lysozyme was codon optimized for expression in yeast and was flanked

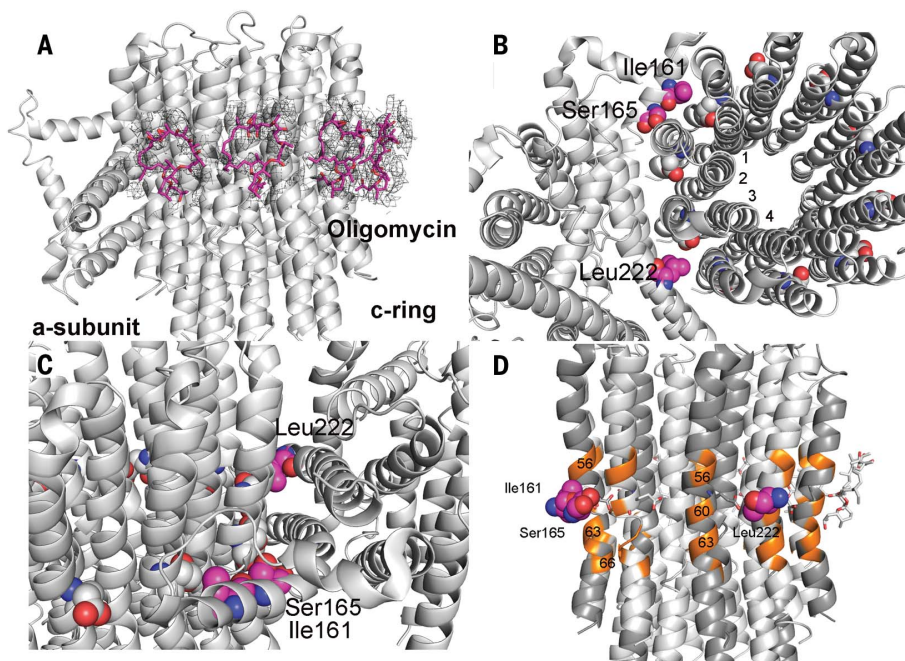


**Fig. 5. Inhibition of the ATP synthase by oligomycin.** (A) Model of oligomycin bound to the  $F_0$ . The electron density (shown at  $4.5 \sigma$ ) fitted with a model of an oligomycin molecule (magenta) at four superimposable positions on the  $c_{10}$ -ring. (B) Positions of residues in the a subunit at which replacements can confer resistance to oligomycin. The three residues Ile<sup>161</sup>, Ser<sup>165</sup>, and Leu<sup>222</sup> in the a subunit are positioned at the interface between subunits  $c^1c^2$  and  $c^3c^4$  and directly in line with cGlu<sup>59</sup> (C) and (D). This position is precisely where oligomycin binds when the site is exposed to the membrane bilayer. (C) Side view of the residues in the a subunit. (D) Positions of residues in c subunits that interact with oligomycin. The c-subunit residues colored orange (Ala<sup>56</sup>, Ala<sup>60</sup>, Leu<sup>63</sup>, Phe<sup>64</sup>, and Leu<sup>66</sup>) are a subset of residues that provide binding interactions with oligomycin (29). (Three of the c subunits are shaded darker gray.)



by two NarI sites that added Gly-Ala to the N and C termini of lysozyme. The assembled gene was used in a “gap repair” reaction to introduce it into the gene encoding the  $\beta$  subunit such that it was inserted just behind the codons encoding the mitochondrial leader peptide on the 5' end and then at the stop codon on the 3' end of the gene, as described (35). The fusion gene was subcloned into the integrating vector, pRS304 (36) and transformed (37) into the yeast strain.

### Biochemistry

We chose to incorporate the yeast ATP synthase into nanodiscs as this is under near native conditions and the oligomycin binding site is at the surface of the  $c_{10}$ -ring in the membrane phase.

Yeast ATP synthase was purified essentially as described except a Co-affinity column was substituted for the Ni-affinity column (33). For reconstitution of the ATP synthase into nanodiscs, the enzyme was purified only through the Co-affinity column.

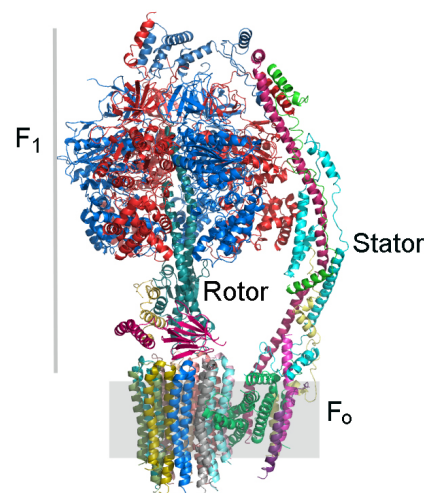
The membrane scaffolding protein (MSP), MSP1E3D1, was expressed in BL21-Gold (DE3) strain (Agilent, Santa Clara, CA) as described (38) with the following changes. After binding to the MSP to the Ni-column, the column was washed with five column volumes of WB (40 mM Tris-Cl, 0.3 M NaCl, 25 mM imidazole, 6 M guanidinium hydrochloride, 5 mM  $\epsilon$ -amino caproic acid and 5 mM benzamidine HCl, 1 mM PMSF, pH 8.0) and then the MSP was eluted with 40 mM Tris-Cl, 0.3 M NaCl, 0.4 M imidazole, 6 M guanidinium hydrochloride, 5 mM  $\epsilon$ -amino caproic acid and 5 mM benzamidine HCl, 1 mM PMSF, pH 8.0. The buffer was exchanged with a HiPrep 26/10 desalting column (GE Healthcare, Uppsala, Sweden) equilibrated with 25 mM Tris-Cl, 0.15 M NaCl, 1 mM EDTA, pH 8.0. The MSP was digested with TEV protease at 30°C for 6 hours [TEV/MSP ratio was 1/100 (mg/mg)]. The TEV digestion reaction mixture was passed through a HiPrep 26/10 desalting column (GE Healthcare, Uppsala, Sweden) equilibrated with WB containing 75 mM imidazole (WBI). The MSP was loaded onto  $Ni^{+2}$ -column equilibrated with WBI. The fractions containing protein that did not bind to the column were collected, pooled together, and dialyzed against storage buffer (25 mM Tris-Cl, 0.1 M NaCl, pH 8.0) at 4°C. The protein concentration of MSP1E3D1, was determined using the extinction coefficient of  $26,930 \text{ M}^{-1} \text{ cm}^{-1}$  at 280 nm (38). MSP1E3D1 was lyophilized and stored at -20°C.

For reconstitution of  $F_1F_0$  into nanodiscs, we used three different lipid preparations. In the case of the structural analysis in the absence of oligomycin, we used nanodiscs prepared from total polar *E. coli* lipids spiked with ergosterol at a ratio of 3:1 on a molar basis, and we also used 1,2-dimyristoyl-*sn*-glycero-3-phosphocholine (DMPC). For the structure in the presence of oligomycin, we used 1-palmitoyl-2-oleoyl-*sn*-glycero-3-phosphocholine (POPC) mixed with cardiolipin (C:18) (CL), at a ratio of 3:1 by weight. The lipids were (obtained from Avanti Polar Lipids, Alabaster, AL) dissolved in chloroform, and stored under argon at -80°C.

The most improved method for reconstitution is reflected in the preparation using POPC:CL. In this procedure, the lipids were added to a glass test tube and the chloroform was removed with a gentle stream of nitrogen. The sample was placed under vacuum for overnight to remove the residual chloroform. The lipids were dissolved in 20 mM Tris-Cl, 0.15 M NaCl, pH 7.4 with 60 mM DDM with the aid of a water bath sonicator. Solubilized lipid was mixed with MSP1E3D1 and  $F_1F_0$  ATP synthase at a molar ratio of 120:15:2.5 (lipid:MSP: $F_1F_0$ ) and the mixture was incubated at 30°C for 1 hour with constant agitation. To initiate nanodisc assembly, Amberlite XAD-2 (Sigma Aldrich, Milwaukee, WI) beads (0.6 g/ml, final) were added and the mix was incubated at 30°C for 24 hours with constant agitation. Adsorbent beads were added in three batches; in first batch 8% of total beads were added and the reaction was incubated for 6 hours; in the second batch, additional 10% of total beads were added and the reaction mix was incubated for another 16 hours; in the final step of addition, the final 82% of total beads were added and the reaction was incubated for another 2 hours. For reconstitution using *E. coli* total polar lipids or DMPC, the adsorbent beads were added in four batches, 25% of the total beads per hour for a total of 4 hours. The beads were removed and the reaction mixture was purified on a Superose-6 (GE Healthcare, Uppsala, Sweden) size exclusion column equilibrated with 20 mM Tris-Cl, 50 mM sucrose, 4 mM  $MgSO_4$ , 1 mM EDTA, 0.25 mM ADP, 0.15 M NaCl, 5 mM  $\epsilon$ -amino caproic acid and 5 mM benzamidine HCl, 1 mM PMSF, pH 8.0. The buffer was exchanged using a centrifugal column (39) (1 ml) using Bio-Gel P-6 (Bio-Rad, Hercules, CA) and buffer containing, 20 mM Tris-Cl, 4 mM  $MgSO_4$ , 1 mM EDTA, 0.25 mM ADP, 0.15 M NaCl, 5 mM  $\epsilon$ -amino caproic acid and 5 mM benzamidine HCl, 1 mM PMSF, pH 8.0. The specific activity (u/mg) and percent oligomycin sensitive ATPase using wild-type enzyme was 10:42, 59:78, and 55:85% for reconstitution using *E. coli* polar lipids, DMPC an POPC/CL, respectively.

### Cryo-electron microscopy data acquisition

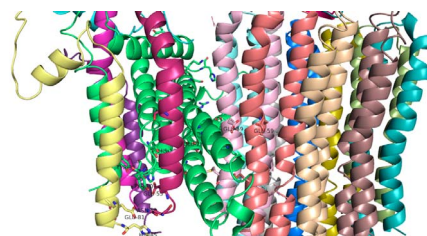
Purified yeast  $F_1F_0$  reconstituted in nanodiscs at the concentration of 1 mg/ml (2.5  $\mu$ l) was applied to a glow-discharged Quantifoil holey carbon grid (1.2/1.3, 400 mesh), and blotted for 3 s with ~91% humidity before plunge-freezing in liquid ethane using a Cryoplunge 3 System (CP3, Gatan). For cryo-EM of  $F_1F_0$  with oligomycin, 60 mM stock solution of oligomycin in dimethyl sulfoxide was added to a final concentration of 30  $\mu$ M, and incubated on ice for 30 min. The mixture (2.5  $\mu$ l) was applied to a grid, blotted and plunge-frozen. Cryo-EM data were recorded on a 300-kV Polara electron microscope (FEI) at Harvard Medical School. All cryo-EM movies were manually recorded with a K2 Summit direct electron detector (Gatan) in super-resolution counting mode using UCSF-Image4 (40). Details of the EM data collection parameters are listed in Table 1.



**Movie 1.** The architecture of the monomeric form of the yeast ATP synthase.



**Movie 2.** Rotation of ATP synthase around the x and y axes.



**Movie 3.** Views of the proton entry pathway and then the proton exit pathway.

## EM image processing

EM data were processed as previously described (41). Dose-fractionated super-resolution movies collected using the K2 Summit direct electron detector were binned over  $2 \times 2$  pixels, and subjected to motion correction using the program MotionCor2 (42). A sum of all frames of each image stack was calculated following a dose-weighting scheme, and used for all image-processing steps except for defocus determination. CTFFIND4 (43) was used to calculate defocus values of the summed images from all movie frames without dose weighting. Particle picking was performed using a semi-automated procedure with SAMUEL and SamViewer (44). Two- and three-dimensional (2D and 3D) classification and 3D refinement were carried out using “relion\_refine\_mpi” in RELION (45). Masked 3D classification focusing on  $F_0$  with residual signal subtraction was performed following a previously described procedure (46). All refinements followed the gold-standard procedure, in which two half data sets were refined independently. The overall resolutions were estimated based on the gold-standard criterion of Fourier shell correlation (FSC) = 0.143. Local resolution variations were estimated from two half data maps using ResMap. The amplitude information of the final maps were corrected by applying a negative B-factor using the program bfactor.exe.

## Model refinement

The initial model was derived from the crystal structure of  $F_1$  ATPase (PDB, 2WPD) and the  $c_{10}$ -ring from our previous crystal structure (PDB 3U2F). Models for subunits OSCP, b, F6, and subunit d were initiated as homology models based on bovine structures (PDB, 2CLY and 5FIK). Models for subunits a, A6L/subunit 8, f, j, and the N-terminal part of subunit b were derived from the cryo-EM structure (PDB 6B2Z). Initial models were rigid-body fitted to our cryo-EM maps, extensively rebuilt in Coot (47), and refined in Refmac (48) using the script *refine\_local*, and subsequently, using real-space refinement in Phenix (49).

Final models were validated with statistics from Ramachandran plots, MolProbity scores, and EMRinger scores (Table 1). MolProbity and EMRinger scores were calculated as described (50, 51).

## Molecular dynamics simulations

All simulations were performed with NAMD2 (52), using CHARMM36 force-field for proteins and lipids (53, 54), periodic boundary conditions, and constant temperature (298 K) and pressure (1 atm). Long-range electrostatic interactions were calculated using PME, with a real-space cut-off of 12 Å. Van der Waals interactions were computed with a Lennard-Jones potential, cut-off at 12 Å with a smooth switching function taking effect at 10 Å. Simulations were carried out for two systems: a complex of the yeast  $c_{10}$ -ring with four oligomycin molecules bound (PDB 4F4S), embedded in a hydrated, pre-equilibrated 1-palmitoyl-2-oleoyl-*sn*-glycero-3-phosphatidyl-

choline (POPC) lipid bilayer; and a system of the same components, with one oligomycin molecule dissociated from the  $c_{10}$ -ring and free in the lipid bilayer. Force-field parameters for oligomycin were derived using the GAAMP server (55). The  $c_{10}$ -ring complex was embedded in the POPC membrane using GRIFFIN (56), as previously described (57). Counter-ions were added to neutralize the charge of the simulation system. The simulation systems were equilibrated following a staged protocol whereby positional and conformational restraints acting of the protein-inhibitor complex are gradually weakened over 200 ns. The equilibrated systems were then used as the starting point for the analysis of the oligomycin binding free energy.

The inhibitor binding free-energy was calculated as  $\Delta G_b = -k_B T \ln N + \Delta G_{\text{int}} + \Delta G_r + \Delta G_t$ , where  $N$  is the number of available binding sites on the  $c_{10}$ -ring,  $\Delta G_{\text{int}}$  is free-energy difference between the associated and dissociated complex, and  $\Delta G_r$  and  $\Delta G_t$  denote the free-energy penalties due to the loss of rotational and translational entropy of the ligand upon binding, respectively ( $k_B$  is the Boltzmann constant and  $T$  the temperature).  $\Delta G_{\text{int}}$  was, in part, derived from calculations of the free-energy change associated with decoupling oligomycin from the rest of the molecular system, in both the bound and unbound states. Analogous calculations were carried out whereby oligomycin is recoupled to the system. These calculations used the Free-Energy Perturbation method, whereby the decoupling and recoupling process is induced through a parameter  $\lambda$  that scales the nonbonded interactions between the ligand and its environment. The parameter  $\lambda$  varied gradually and step-wise between 1 and 0, and vice versa, in 54 consecutive simulations. For each value of  $\lambda$ , in either direction, an incremental free-energy change was estimated from a simulation of 1 ns, after a 200-ps equilibration stage, in the case of bound oligomycin; for the dissociated ligand, the sampling and equilibration times per intermediate were 1.5 ns and 300 ps, respectively. The resulting values for this decoupling free-energy are 39.8 and 32.8 kcal/mol for the bound and unbound ligand, respectively. Intramolecular interactions thus result in a free-energy contribution that favors binding, i.e.,  $\Delta \Delta G_{\text{FEP}} = -7.0$  kcal/mol.

For computational efficiency, during the above-mentioned decoupling/recoupling simulations, the internal conformation of the oligomycin molecule considered was preserved using a harmonic RMSD restraint, defined relative to that in the equilibrated systems, with a force constant  $k = 9.6$  kcal/mol Å<sup>2</sup>. Hence,  $\Delta G_{\text{int}} = \Delta \Delta G_{\text{FEP}} + \Delta \Delta G_{\text{RMSD}}$ , where the latter term is the difference in the free-energy cost of imposing the conformational restraint on the bound versus the unbound ligand. This contribution was computed separately, through an additional set of simulations whereby  $k$  is scaled down gradually, using a parameter  $\alpha$  that varies step-wise from 1 to 0, and vice versa. Specifically, 50 simulations of 1 ns each were carried out in each direction for the bound and unbound states. From each of

these simulation series, the value of  $\Delta G_{\text{RMSD}}$  can be derived using the expressions:

$$\Delta G_{\text{RMSD}} = -k_B T \sum_{w=1}^{W=50} \ln \left\langle \exp \left\{ -\frac{\Delta U_w(t)}{k_B T} \right\} \right\rangle$$

$$\Delta U_w(t) = \frac{1}{2} k (\alpha_{w+1} - \alpha_w) \text{RMSD}(t)^2$$

where  $\langle \dots \rangle$  denotes a time-average. The calculated values of  $\Delta G_{\text{RMSD}}$  are 0.5 and 0.9 kcal/mol for the bound and unbound ligand, respectively; that is,  $\Delta \Delta G_{\text{RMSD}} = 0.4$  kcal/mol, i.e., binding is only marginally disfavored due to loss of conformational dynamics of the inhibitor. The resulting value of  $\Delta G_{\text{int}}$  is thus  $-6.6$  kcal/mol.

When dissociated from the  $c_{10}$ -ring, oligomycin adopts primarily an upright orientation, i.e., its rotational freedom relative to the membrane plane is restricted; however, the molecule rotates freely around the membrane perpendicular. The free-energy cost associated with the loss of rotational entropy upon binding can be therefore estimated as  $\Delta G_r = -k_B T \ln[\Delta\theta/2\pi]$ , where  $\Delta\theta$  is the rotational fluctuation of the bound ligand perpendicularly to the membrane; from our simulations we estimate that  $\Delta\theta \sim 0.44$  rad (or 25 degrees), and thus  $\Delta G_r = 1.6$  kcal/mol.

Similarly, to estimate the free-energy cost associated with the loss of translational entropy upon binding, we used the expression  $\Delta G_t = -k_B T \ln[D^0 \Delta A]$ , where  $\Delta A$  represents the translational freedom of the bound ligand on the membrane plane when bound to the protein, whereas  $D^0$  is the ligand area-density in the surrounding medium, akin to the standard concentration  $C^0$  used in the context of three-dimensional bi-molecular association. Although there is no analogous standard for  $D^0$ , the mole fraction of the inhibitor in the lipid membrane may be used to define a reference state. For example, an assumed mole fraction of 0.01, i.e., 1 inhibitor per 100 lipids, translates into  $D^0 = 7,000$  Å<sup>2</sup>, for an area-per-lipid of  $\sim 70$  Å<sup>2</sup>. From our simulations we estimate that  $\Delta A = 4$  Å<sup>2</sup>, and therefore an oligomycin mole fraction of 0.01 implies  $\Delta G_t = 4.4$  kcal/mol.

## Primary sequence analysis

Primary sequence alignment was done using COBALT (58).

## Figure images

Many of the images presented in the figures were made with the assistance of Pymol (59).

## REFERENCES AND NOTES

1. T. Xu, V. Pagadala, D. M. Mueller, Understanding structure, function, and mutations in the mitochondrial ATP synthase. *Microb. Cell* 2, 105–125 (2015). doi: 10.15698/mic2015.04.197; pmid: 25938092
2. I. Arnold, K. Pfeiffer, W. Neupert, R. A. Stuart, H. Schagger, Yeast mitochondrial  $F_1F_0$ -ATP synthase exists as a dimer: Identification of three dimer-specific subunits. *EMBO J.* 17, 7170–7178 (1998). doi: 10.1093/emboj/17.24.7170; pmid: 9857174
3. B. Daum, D. Nicastro, J. Austin II, J. R. McIntosh, W. Kühlbrandt, Arrangement of photosystem II and ATP synthase in chloroplast membranes of spinach and pea. *Plant Cell* 22, 1299–1312 (2010). doi: 10.1105/tpc.109.071431; pmid: 20388855



4. L. A. Baker, I. N. Watt, M. J. Runswick, J. E. Walker, J. L. Rubinstein, Arrangement of subunits in intact mammalian mitochondrial ATP synthase determined by cryo-EM. *Proc. Natl. Acad. Sci. U.S.A.* **109**, 11675–11680 (2012). doi: [10.1073/pnas.1204935109](#); pmid: [22753497](#)
5. I. G. Denisov, Y. V. Grinkova, A. A. Lazarides, S. G. Sligar, Directed self-assembly of monodisperse phospholipid bilayer nanodiscs with controlled size. *J. Am. Chem. Soc.* **126**, 3477–3487 (2004). doi: [10.1021/ja0393574](#); pmid: [15025475](#)
6. J. P. Abrahams, A. G. W. Leslie, R. Lutter, J. E. Walker, Structure at 2.8 Å resolution of F<sub>1</sub>-ATPase from bovine heart mitochondria. *Nature* **370**, 621–628 (1994). doi: [10.1038/370621a0](#); pmid: [8065448](#)
7. V. Kabaleeswaran, N. Puri, J. E. Walker, A. G. Leslie, D. M. Mueller, Novel features of the rotary catalytic mechanism revealed in the structure of yeast F<sub>1</sub> ATPase. *EMBO J.* **25**, 5433–5442 (2006). doi: [10.1038/sj.emboj.7601410](#); pmid: [17082766](#)
8. A. Dautant, J. Velours, M. F. Giraud, Crystal structure of the Mg-ADP-inhibited state of the yeast F<sub>1</sub>ATP synthase. *J. Biol. Chem.* **285**, 29502–29510 (2010). doi: [10.1074/jbc.M110.124529](#); pmid: [20610387](#)
9. D. Stock, A. G. W. Leslie, J. E. Walker, Molecular architecture of the rotary motor in ATP synthase. *Science* **286**, 1700–1705 (1999). doi: [10.1126/science.286.5445.1700](#); pmid: [10576729](#)
10. V. K. Dickson, J. A. Silvester, I. M. Fearnley, A. G. Leslie, J. E. Walker, On the structure of the stator of the mitochondrial ATP synthase. *EMBO J.* **25**, 2911–2918 (2006). doi: [10.1038/sj.emboj.7601177](#); pmid: [16791136](#)
11. H. Guo, S. A. Bueler, J. L. Rubinstein, Atomic model for the dimeric F<sub>3</sub> region of mitochondrial ATP synthase. *Science* **358**, 936–940 (2017). doi: [10.1126/science.1254815](#); pmid: [29074581](#)
12. K. R. Vinothkumar, M. G. Montgomery, S. Liu, J. E. Walker, Structure of the mitochondrial ATP synthase from *Pichia angusta* determined by electron cryo-microscopy. *Proc. Natl. Acad. Sci. U.S.A.* **113**, 12709–12714 (2016). doi: [10.1073/pnas.1615902113](#); pmid: [27791192](#)
13. S. B. Vik, J. C. Long, T. Wada, D. Zhang, A model for the structure of subunit a of the *Escherichia coli* ATP synthase and its role in proton translocation. *Biochim. Biophys. Acta* **1458**, 457–466 (2000). doi: [10.1016/S0005-2728\(00\)00094-3](#); pmid: [10838058](#)
14. S. B. Vik, B. J. Antonio, A mechanism of proton translocation by F<sub>1</sub>F<sub>0</sub> ATP synthases suggested by double mutants of the a subunit. *J. Biol. Chem.* **269**, 30364–30369 (1994). pmid: [7982950](#)
15. W. Junge, H. Lill, S. Engelbrecht, ATP synthase: An electrochemical transducer with rotatory mechanics. *Trends Biochem. Sci.* **22**, 420–423 (1997). doi: [10.1016/S0968-0004\(97\)00129-8](#); pmid: [9397682](#)
16. J. Symersky et al., Structure of the c<sub>10</sub> ring of the yeast mitochondrial ATP synthase in the open conformation. *Nat. Struct. Mol. Biol.* **19**, 485–491, S1 (2012). doi: [10.1038/nsmb.2284](#); pmid: [22504883](#)
17. D. Pogoryelov, O. Yildiz, J. D. Faraldo-Gómez, T. Meier, High-resolution structure of the rotor ring of a proton-dependent ATP synthase. *Nat. Struct. Mol. Biol.* **16**, 1068–1073 (2009). doi: [10.1038/nsmb.1678](#); pmid: [19783985](#)
18. N. Mitome et al., Essential arginine residue of the F<sub>0</sub>-1 subunit in F<sub>1</sub>F<sub>0</sub>-ATP synthase has a role to prevent the proton shortcut without c-ring rotation in the F<sub>0</sub> proton channel. *Biochem. J.* **430**, 171–177 (2010). doi: [10.1042/BJ20100621](#); pmid: [20518749](#)
19. N. Klusch, B. J. Murphy, D. J. Mills, Ö. Yildiz, W. Kühlbrandt, Structural basis of proton translocation and force generation in mitochondrial ATP synthase. *eLife* **6**, e33274 (2017). doi: [10.7554/eLife.33274](#); pmid: [29210357](#)
20. M. Allegretti et al., Horizontal membrane-intrinsic α-helices in the stator a-subunit of an F-type ATP synthase. *Nature* **521**, 237–240 (2015). doi: [10.1038/nature14185](#); pmid: [25707805](#)
21. V. Leone, J. D. Faraldo-Gómez, Structure and mechanism of the ATP synthase membrane motor inferred from quantitative integrative modeling. *J. Gen. Physiol.* **148**, 441–457 (2016). doi: [10.1085/jgp.201611679](#); pmid: [27821609](#)
22. F. M. Assadi-Porter, R. H. Fillingame, Proton-translocating carboxyl of subunit c of F<sub>1</sub>F<sub>0</sub> H<sup>+</sup>-ATP synthase: The unique environment suggested by the pK<sub>a</sub> determined by <sup>1</sup>H NMR. *Biochemistry* **34**, 16186–16193 (1995). doi: [10.1021/bi00049a034](#); pmid: [8519776](#)
23. M. J. Root, R. MacKinnon, Two identical noninteracting sites in an ion channel revealed by proton transfer. *Science* **265**, 1852–1856 (1994). doi: [10.1126/science.7522344](#); pmid: [7522344](#)
24. J. A. Morrill, R. MacKinnon, Isolation of a single carboxyl-carboxylate proton binding site in the pore of a cyclic nucleotide-gated channel. *J. Gen. Physiol.* **114**, 71–84 (1999). doi: [10.1085/jgp.114.1.71](#); pmid: [10398693](#)
25. T. K. Harris, G. J. Turner, Structural basis of perturbed pK<sub>a</sub> values of catalytic groups in enzyme active sites. *ILBMB Life* **53**, 85–98 (2002). doi: [10.1080/1521654021468](#); pmid: [12049200](#)
26. R. E. Koeppe II, R. M. Stroud, Mechanism of hydrolysis by serine proteases: Direct determination of the pK<sub>a</sub>'s of aspartyl-102 and aspartyl-194 in bovine trypsin using difference infrared spectroscopy. *Biochemistry* **15**, 3450–3458 (1976). doi: [10.1021/bi00661a009](#); pmid: [986162](#)
27. F. I. Valiyaveetil, R. H. Fillingame, On the role of Arg-210 and Glu-219 of subunit a in proton translocation by the *Escherichia coli* F<sub>0</sub>F<sub>1</sub>-ATP synthase. *J. Biol. Chem.* **272**, 32635–32641 (1997). doi: [10.1074/jbc.272.51.32635](#); pmid: [9405480](#)
28. F. I. Valiyaveetil, R. H. Fillingame, Transmembrane topography of subunit a in the *Escherichia coli* F<sub>0</sub>F<sub>1</sub> ATP synthase. *J. Biol. Chem.* **273**, 16241–16247 (1998). doi: [10.1074/jbc.273.26.16241](#); pmid: [9632683](#)
29. J. Symersky, D. Osowski, D. E. Walters, D. M. Mueller, Oligomycin frames a common drug-binding site in the ATP synthase. *Proc. Natl. Acad. Sci. U.S.A.* **109**, 13961–13965 (2012). doi: [10.1073/pnas.1207912109](#); pmid: [22869738](#)
30. U. P. John, P. Nagley, Amino acid substitutions in mitochondrial ATPase subunit 6 of *Saccharomyces cerevisiae* leading to oligomycin resistance. *FEBS Lett.* **207**, 79–83 (1986). doi: [10.1016/0014-5793\(86\)80016-3](#); pmid: [2876917](#)
31. I. G. Denisov, B. J. Baas, Y. V. Grinkova, S. G. Sligar, Cooperativity in cytochrome P450 3A4: Linkages in substrate binding, spin state, uncoupling, and product formation. *J. Biol. Chem.* **282**, 7066–7076 (2007). doi: [10.1074/jbc.M609589200](#); pmid: [17213193](#)
32. R. B. Kapust et al., Tobacco etch virus protease: Mechanism of autolysis and rational design of stable mutants with wild-type catalytic proficiency. *Protein Eng.* **14**, 993–1000 (2001). doi: [10.1093/protein/14.12.993](#); pmid: [11809930](#)
33. V. Pagadala, L. Vistain, J. Symersky, D. M. Mueller, Characterization of the mitochondrial ATP synthase from yeast *Saccharomyces cerevisiae*. *J. Bioenerg. Biomembr.* **43**, 333–347 (2011). doi: [10.1007/s10863-011-9364-5](#); pmid: [21748405](#)
34. U. Güldener, S. Heck, T. Fielder, J. Beinhauer, J. H. Hegemann, A new efficient gene disruption cassette for repeated use in budding yeast. *Nucleic Acids Res.* **24**, 2519–2524 (1996). doi: [10.1093/nar/24.13.2519](#); pmid: [8692690](#)
35. N. Puri, J. Lai-Zhang, S. Meier, D. M. Mueller, Expression of bovine F<sub>1</sub>-ATPase with functional complementation in yeast *Saccharomyces cerevisiae*. *J. Biol. Chem.* **280**, 22418–22424 (2005). doi: [10.1074/jbc.M41113200](#); pmid: [15817482](#)
36. R. S. Sikorski, P. Hieter, A system of shuttle vectors and yeast host strains designed for efficient manipulation of DNA in *Saccharomyces cerevisiae*. *Genetics* **122**, 19–27 (1989). pmid: [2659436](#)
37. R. D. Gietz, R. A. Woods, Transformation of yeast by lithium acetate/single-stranded carrier DNA/polyethylene glycol method. *Methods Enzymol.* **350**, 87–96 (2002). doi: [10.1016/S0076-6879\(02\)50957-5](#); pmid: [12073338](#)
38. T. K. Ritchie et al., Chapter Eleven - Reconstitution of membrane proteins in phospholipid bilayer nanodiscs. *Methods Enzymol.* **464**, 211–231 (2009). doi: [10.1016/S0076-6879\(09\)64011-8](#); pmid: [19903557](#)
39. H. S. Penefsky, A centrifuged-column procedure for the measurement of ligand binding by beef heart F<sub>1</sub>. *Methods Enzymol.* **56**, 527–530 (1979). doi: [10.1016/0076-6879\(79\)56050-9](#); pmid: [156867](#)
40. X. Li, S. Zheng, D. A. Agard, Y. Cheng, Asynchronous data acquisition and on-the-fly analysis of dose fractionated cryoEM images by UCSFImage. *J. Struct. Biol.* **192**, 174–178 (2015). doi: [10.1016/j.jsb.2015.09.003](#); pmid: [26370395](#)
41. W. Mi et al., Structural basis of MsaA-mediated lipopolysaccharide transport. *Nature* **549**, 233–237 (2017). doi: [10.1038/nature23649](#); pmid: [28869968](#)
42. S. Q. Zheng et al., MotionCor2: Anisotropic correction of beam-induced motion for improved cryo-electron microscopy. *Nat. Methods* **14**, 331–332 (2017). doi: [10.1038/nmeth.4193](#); pmid: [28250466](#)
43. A. Rohou, N. Grigorieff, CTFFIND4: Fast and accurate defocus estimation from electron micrographs. *J. Struct. Biol.* **192**, 216–221 (2015). doi: [10.1016/j.jsb.2015.08.008](#); pmid: [26278980](#)
44. H. Ru et al., Molecular mechanism of V(D)J recombination from synaptic RAG1-RAG2 complex structures. *Cell* **163**, 1138–1152 (2015). doi: [10.1016/j.cell.2015.10.055](#); pmid: [26548953](#)
45. S. H. Scheres, RELION: Implementation of a Bayesian approach to cryo-EM structure determination. *J. Struct. Biol.* **180**, 519–530 (2012). doi: [10.1016/j.jsb.2012.09.006](#); pmid: [23000701](#)
46. X. C. Bai, E. Rajendra, G. Yang, Y. Shi, S. H. Scheres, Sampling the conformational space of the catalytic subunit of human γ-secretase. *eLife* **4**, e11182 (2015). doi: [10.7554/eLife.11182](#); pmid: [26623517](#)
47. P. Emsley, K. Cowtan, Coot: Model-building tools for molecular graphics. *Acta Crystallogr. D Biol. Crystallogr.* **60**, 2126–2132 (2004). doi: [10.1107/S0907444904019158](#); pmid: [15572765](#)
48. G. N. Murshudov et al., REFMAC5 for the refinement of macromolecular crystal structures. *Acta Crystallogr. D Biol. Crystallogr.* **67**, 355–367 (2011). doi: [10.1107/S0907444911001314](#); pmid: [21460454](#)
49. P. D. Adams et al., PHENIX: A comprehensive Python-based system for macromolecular structure solution. *Acta Crystallogr. D Biol. Crystallogr.* **66**, 213–221 (2010). doi: [10.1107/S09074449090052925](#); pmid: [20124702](#)
50. B. A. Barad et al., EMRinger: Side chain-directed model and map validation for 3D cryo-electron microscopy. *Nat. Methods* **12**, 943–946 (2015). doi: [10.1038/nmeth.3541](#); pmid: [26280328](#)
51. V. B. Chen et al., MolProbity: All-atom structure validation for macromolecular crystallography. *Acta Crystallogr. D Biol. Crystallogr.* **66**, 12–21 (2010). doi: [10.1107/S09074449090042073](#); pmid: [20057044](#)
52. J. C. Phillips et al., Scalable molecular dynamics with NAMD. *J. Comput. Chem.* **26**, 1781–1802 (2005). doi: [10.1002/jcc.20289](#); pmid: [16222654](#)
53. R. B. Best et al., Optimization of the additive CHARMM all-atom protein force field targeting improved sampling of the backbone φ, ψ and side-chain χ<sub>1</sub> and χ<sub>2</sub> dihedral angles. *J. Chem. Theory Comput.* **8**, 3257–3273 (2012). doi: [10.1021/ct300400x](#); pmid: [23341755](#)
54. J. B. Klauda et al., Update of the CHARMM all-atom additive force field for lipids: Validation on six lipid types. *J. Phys. Chem. B* **114**, 7830–7843 (2010). doi: [10.1021/jp101759q](#); pmid: [20496934](#)
55. L. Huang, B. Roux, Automated force field parameterization for non-polarizable and polarizable atomic models based on ab initio target data. *J. Chem. Theory Comput.* **9**, 3543–3556 (2013). doi: [10.1021/ct4003477](#); pmid: [24223528](#)
56. R. Staritzbichler, C. Anselmi, L. R. Forrest, J. D. Faraldo-Gómez, GRIFIN: A versatile methodology for optimization of protein-lipid interfaces for membrane protein simulations. *J. Chem. Theory Comput.* **7**, 1167–1176 (2011). doi: [10.1021/ct100576m](#); pmid: [24707727](#)
57. W. Zhou, V. Leone, A. Krah, J. D. Faraldo-Gómez, Predicted structures of the proton-bound membrane-embedded rotor rings of the *Saccharomyces cerevisiae* and *Escherichia coli* ATP synthases. *J. Phys. Chem. B* **121**, 3297–3307 (2017). doi: [10.1021/acs.jpcb.6b08051](#); pmid: [27715045](#)
58. J. S. Papadopoulos, R. Agarwal, COBAL: Constraint-based alignment tool for multiple protein sequences. *Bioinformatics* **23**, 1073–1079 (2007). doi: [10.1093/bioinformatics/btm076](#); pmid: [17332019](#)
59. The PyMOL Molecular Graphics System, version 2.0, Schrödinger, LLC.

## ACKNOWLEDGMENTS

Many thanks to J. Rubinstein for providing a copy of his manuscript and the model for yeast F<sub>0</sub> before publication. **Funding:** The work was supported by a grant from NIH, R01GM066223, to D.M.M. W.Z. and J.D.F.-G. are funded by the Division of Intramural Research of the National Heart, Lung, and Blood Institute. **Author contributions:** A.P.S. designed and performed the biochemical experiments; M.Lu. performed EM data collection and image processing; W.Z. performed the molecular dynamics simulation studies; J.S. helped in the atomic model building and refinement; D.B. helped with the design and performed biochemical experiments; M.G.C. helped with the cryo-EM experiments; J.D.F.-G. designed and supervised the molecular dynamics simulation studies; and M.Li. supervised the EM studies. D.M.M. devised and supervised experiments and analyzed data. A.P.S., M.Lu., W.Z., J.S., D.B., J.D.F.-G., M.Li., and D.M.M. helped with writing the manuscript. **Competing interests:** None declared. **Data and materials availability:** Four 3D cryo-EM density maps of the yeast mitochondrial ATP synthase in nanodiscs have been deposited in the Electron Microscopy Data Bank under accession numbers EMD-7548 (F<sub>1</sub>F<sub>0</sub>), EMD-7549 (F<sub>0</sub>), EMD-7546 (F<sub>0</sub> with oligomycin), and EMD-7547 (F<sub>0</sub> with oligomycin). The corresponding atomic coordinates for the atomic models have been deposited in the Protein Data Bank under accession numbers 6CP6 (F<sub>1</sub>F<sub>0</sub>), 6CP7 (F<sub>0</sub>), 6CP3 (F<sub>1</sub>F<sub>0</sub> with oligomycin), and 6CP5 (F<sub>0</sub> with oligomycin). Correspondence and requests for materials should be addressed to the corresponding authors.

## SUPPLEMENTARY MATERIALS

[www.sciencemag.org/content/360/6389/eaas9699/suppl/DC1](http://www.sciencemag.org/content/360/6389/eaas9699/suppl/DC1)  
Supplementary Text  
Figs. S1 to S12  
References

15 January 2018; accepted 30 March 2018  
Published online 12 April 2018  
10.1126/science.aas9699

## High-resolution cryo-EM analysis of the yeast ATP synthase in a lipid membrane

Anurag P. Srivastava, Min Luo, Wenchang Zhou, Jindrich Symersky, Dongyang Bai, Melissa G. Chambers, José D. Faraldo-Gómez, Maofu Liao and David M. Mueller

*Science* **360** (6389), eaas9699.

DOI: 10.1126/science.aas9699originally published online April 12, 2018

### Protons find a path

Adenosine triphosphate (ATP) synthases are dynamos that interconvert rotational and chemical energy. Capturing the complete structure of these multisubunit membrane-bound complexes has been hindered by their inherent ability to adopt multiple conformations. Srivastava *et al.* used protein engineering to freeze mitochondrial ATP synthase from yeast in a single conformation and obtained a structure with the inhibitor oligomycin, which binds to the rotating c-ring within the membrane. Hahn *et al.* show that chloroplast ATP synthase contains a built-in inhibitor triggered by oxidizing conditions in the dark chloroplast. The mechanisms by which these machines are powered are remarkably similar: Protons are shuttled through a channel to the membrane-embedded c-ring, where they drive nearly a full rotation of the rotor before exiting through another channel on the opposite side of the membrane (see the Perspective by Kane).

*Science*, this issue p. eaas9699, p. eaat4318; see also p. 600

#### ARTICLE TOOLS

<http://science.sciencemag.org/content/360/6389/eaas9699>

#### SUPPLEMENTARY MATERIALS

<http://science.sciencemag.org/content/suppl/2018/04/11/science.aas9699.DC1>

#### RELATED CONTENT

<http://science.sciencemag.org/content/sci/360/6389/600.full>  
<http://science.sciencemag.org/content/sci/360/6389/eaat4318.full>

#### REFERENCES

This article cites 58 articles, 20 of which you can access for free  
<http://science.sciencemag.org/content/360/6389/eaas9699#BIBL>

#### PERMISSIONS

<http://www.sciencemag.org/help/reprints-and-permissions>

Use of this article is subject to the [Terms of Service](#)